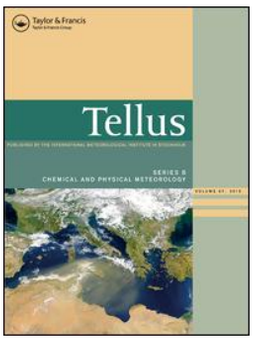

Tellus B: Chemical and Physical Meteorology

ISSN: (Print) 1600-0889 (Online) Journal homepage: https://www.tandfonline.com/loi/zelb20

Impact of vertical resolution on the transport of passive tracers in the ECHAM4 model

C. Land, J. Feichter & R. Sausen

To cite this article: C. Land, J. Feichter & R. Sausen (2002) Impact of vertical resolution on the transport of passive tracers in the ECHAM4 model, Tellus B: Chemical and Physical Meteorology, 54:4, 344-360, DOI: 10.3402/tellusb.v54i4.16670

To link to this article: https://doi.org/10.3402/tellusb.v54i4.16670

© 2002 The Author(s). Published by Taylor & Francis.

Published online: 15 Dec 2016.

Submit your article to this journal

Article views: 29

Citing articles: 5 View citing articles

Full Terms & Conditions of access and use can be found at
https://www.tandfonline.com/action/journalInformation?journalCode=zelb20

Tellus (2002), 54B, 344–360
Printed in UK. All rights reserved

Copyright © Blackwell Munksgaard, 2002
TELLUS
ISSN 0280–6509

Impact of vertical resolution on the transport of passive tracers in the ECHAM4 model

By C. LAND[1]*, J. FEICHTER[1] and R. SAUSEN[2], [1]*Max-Planck-Institut für Meteorologie, Bundesstraße 55, D-20146 Hamburg, Germany;* [2]*Institut für Physik der Atmosphäre, DLR Oberpfaffenhofen, D-82234 Wessling, Germany*

(Manuscript received 2 July 2001; in original form 21 May 2002)

ABSTRACT

The transport of the passive tracers $^{14}CO_2$ and SF_6 has been modelled with two versions of the general circulation model ECHAM4 with different vertical resolutions: the standard model with 19 model layers (L19) and a higher-resolution version with 39 layers (L39). We study the impact of vertical resolution on the modelled transport characteristics. Both models are able to capture the observed SF_6 concentrations in the troposphere, but in the stratosphere the SF_6 mixing ratios are overestimated. L39 generally calculates higher stratospheric SF_6 mixing ratios than L19. This deviation increases with altitude. The difference between the modelled profiles is partly attributed to the residual mean meridional circulation, which is stronger in L39 than in L19, and partly to the initial globally constant SF_6 concentration. The comparison of modelled $^{14}CO_2$ surface concentrations and vertical profiles with observations has shown that an increased vertical resolution in the climate model ECHAM4 reduces the strength of stratosphere–troposphere exchange. L39 allows a better representation of sharp gradients at the tropopause than L19. This results in a weaker downward transport across the tropopause. However, compared to observations the downward transport is still too strong even in the L39 simulation.

1. Introduction

The global model ECHAM4 has been established as a powerful tool for global climate variability and change simulations (e.g. Sausen et al., 1997; Roeckner et al., 1999), for climate sensitivity experiments (e.g. Feichter and Lohmann, 1997), and for tracer transport studies (e.g. Timmreck et al., 1999; Kjellström et al., 2000). However, characteristic shortcomings have shown up concerning the transport of chemical species and passive tracers in the model's stratosphere and upper troposphere. Timmreck et al. (1999), who modelled the eruption of the volcano Mount Pinatubo and the subsequent transport of volcanic aerosol, have shown that sulfate is transported poleward and downward into the model's troposphere at a rate much faster than observed. Kjellström et al. (2000) supported this finding in their transport study of $^{14}CO_2$, the oxidant of radiocarbon (^{14}C). They simulated the spreading of $^{14}CO_2$, which was introduced into the stratosphere of the northern hemisphere by above-ground nuclear weapon tests in the fifties and in the beginning of the sixties. They found that the modelled $^{14}CO_2$ concentration at surface stations increased faster than observed during the first year after the nuclear test ban treaty.

Insufficient vertical and horizontal resolution may be blamed for a substantial part of the deficient transport characteristics in the ECHAM4 model studies cited above. Sharp gradients, as are observed for dynamic parameters like potential vorticity close to the tropopause, cannot be reproduced with the large grid box sizes typical for current GCMs. Additionally, the numerical diffusion associated with the semi-Lagrangian transport scheme used for the tracer transport is probably too strong. Enhanced spatial resolution can be expected to decrease the problems in both respects (Rasch and Lawrence, 1998).

*Corresponding author.
e-mail: land@dkrz.de

So far efforts in improving large-scale dynamics have mainly focussed on increasing the horizontal resolution (e.g. Boville, 1991; Senior, 1995; Williamson et al., 1995; Marshall et al., 1997), developing more sophisticated parametrisation schemes (e.g. Lohmann and Roeckner, 1996), or different transport schemes (e.g. Rasch and Lawrence, 1998; Reithmeier and Sausen, 2002). Relatively little attention has been paid to the sensitivity of simulated dynamics on the vertical resolution, although Lindzen and Fox-Rabinovitz (1989) explained that the vertical resolution has to be chosen dynamically consistent to the horizontal resolution in order to improve the quality of the model output. Their findings were supported by Olga et al. (1991). Also Tsuyuki (1994) showed that a higher vertical resolution in the stratosphere is necessary to improve the simulated tropospheric variability. However, Boville (1991) detected only minor changes as he reduced the vertical grid spacing from 2.8 to 0.7 km at a horizontal spectral resolution of T21. Tompkins and Emanuel (2000) pointed out that GCMs need a vertical resolution of at least 25 hPa to attain numerical convergence in simulated water-vapour distribution.

The impact of the horizontal and vertical resolution on simulated climate statistics has already been studied with ECHAM4.L19 (hereafter abbreviated L19) and ECHAM4.L39(DLR) (hereafter abbreviated L39), a version of ECHAM4 with higher vertical resolution (Stendel and Roeckner, 1998; Land et al., 1999, respectively). However, these studies did not examine the sensitivity of the tracer transport in ECHAM4 to an increased vertical resolution. Austin et al. (1997) were able to improve the ozone distribution in their GCM simulations by increasing the number of vertical levels from 19 to 49, mainly in the tropopause region. Pope et al. (2001) substantially improved the simulated water vapour and temperature distribution in the Met Office Climate model by increasing the number of model layers from 19 to 30. In this study we use the passive tracers sulfur hexafluoride (SF_6) and excess $^{14}CO_2$, namely $^{14}CO_2$ that was introduced into the atmosphere by above-ground nuclear weapon tests, to assess the impact of an increased vertical resolution on the simulated tracer transport.

SF_6 and excess $^{14}CO_2$ are valuable tracers for atmospheric and hydrological dynamics, because they are very stable and can be measured with high accuracy (Hesshaimer et al., 1994; Maiss et al., 1996; Upstillgoddard and Wilkins, 1998). SF_6 is an anthropogenic trace gas with a lifetime of about 3200 yr. It is predominantly used as an insulating gas in high-voltage electrical equipment, but also as a cover gas in the metal processing industries. It escapes to the atmosphere through leaks and during repair or servicing (Ko et al., 1993). SF_6 has already been used to evaluate model dynamics in terms of stratosphere–troposphere exchange (Kjellström et al., 2000) and transport time scales (Manzini and Feichter, 1999; Waugh et al., 1997), and to compare the transport characteristics of several global models (Denning et al., 1999). The radioactive isotope carbon-14 (^{14}C) is naturally produced by interaction of neutrons with atmospheric nitrogen in the upper atmosphere. However, due to the above-ground nuclear weapon tests of the late 1950s and 1960s the atmospheric ^{14}C level increased substantially. In 1963 the northern hemisphere surface concentration was twice the background value (Nydal and Lövseth, 1983). ^{14}C has a half-life of 5730 yr. In the atmosphere it is rapidly oxidised to form $^{14}CO_2$ which is incorporated in the global carbon cycle. ^{14}C has been used to study stratosphere dynamics in two-dimensional (2D) models (e.g. Johnston, 1989; Kinnison et al., 1993; Shia et al., 1993) and to analyse the carbon exchange between the atmosphere and the oceans (Hesshaimer et al., 1994).

2. Model description

The global model ECHAM4 was developed from the weather forecast model of the European Centre for Medium-Range Weather Forecasts (ECMWF). It is a spectral model based on the primitive equations. The prognostic variables are the logarithm of surface pressure, temperature, vorticity and divergence of the horizontal wind, water vapour, and liquid water mixing ratio. In addition a number of passive tracers can be transported. Water vapour, cloud water, and tracers are advected by a semi-Lagrangian scheme (based on Williamson and Rasch, 1989, 1994), while the remaining prognostic variables are transported by the Eulerian (spectral) advection scheme. A horizontal spectral resolution of T30 is used for the current study, corresponding to an isotropic resolution of about 6° for dynamics. The semi-Lagrangian scheme and the parametrised physical processes are calculated on the associated Gaussian transform grid of approximately $3.75^\circ \times 3.75^\circ$ in latitude and longitude. The semi-implicit leap-frog time-stepping scheme employs a time step of 30 min. The model contains a state-of-the-art parametrisation package for unresolved dynamical and physical processes, including radiation,

cumulus convection, stratiform clouds, gravity wave drag, vertical turbulent diffusion and surface fluxes, land surface processes, and horizontal diffusion. The characteristics of the ECHAM4 standard model are described comprehensively by Roeckner et al. (1996), and ECHAM4 features that were adopted from previous ECHAM versions or from the original ECMWF forecast model can be found in Roeckner et al. (1992) and Simmons et al. (1989), respectively.

The atmosphere general circulation model L39 was derived from the operational ECHAM4 model. While the standard ECHAM4 uses 19 vertical levels, L39 vertically resolves the model atmosphere with 39 layers in a hybrid σ–p coordinate system. The top layer of both models is centred at 10 hPa (about 30 km). The highest increase in vertical levels has been achieved in the upper troposphere and above, e.g. the layer depth in the tropopause region has been reduced from 2.0 to 0.7 km. In contrast to L19, the L39 model has roughly consistent resolution away from the Equator according to Lindzen and Fox-Rabinovitz (1989). Further, Boville and Randel (1992) investigated equatorial waves with a stratospheric GCM. They found that vertical grid spacings of about 1 km or less appear to be required at a horizontal spectral resolution of T21 to represent these waves adequately. Thus, the vertical resolution increase of L19 to L39 does make sense at T30. L39 was tuned independently from the 19 layer version in order to account for the effect of parametrisations that depend on the layer thickness, i.e. some free parameters in the cloud physics parametrisation scheme had to be adapted to the reduced layer thickness in order to restore the long-term mean radiative balance at the top of the model atmosphere. Thus a meaningful comparison of the L39 and L19 results was possible. The details of the tuning process are given in Land et al. (1999). This report also provides a detailed model description and compares the main features of the climatologies simulated with both model versions at T30 horizontal spectral resolution. Only a few variables are sensitive to a change in vertical resolution. Fractional cloud coverage is significantly reduced in L39, particularly in the upper troposphere. The overall reduction of cloud coverage in L39 relative to L19 is a direct consequence of the vertical resolution change, as the threshold value for upper level cloud formation in the stratiform cloud scheme had to be increased. The variability of temperature and zonal wind on daily and weekly time scales is substantially enhanced above 50 hPa due to stronger eddy activity. The latter feature is of importance for the study presented here. The residual mean meridional circulation, which may be regarded as a suggestive predictor of the model's transport characteristics, is stronger the higher the vertical and meridional gradients of eddy heat flux at a given vertical temperature gradient (Andrews et al., 1987). The residual mean meridional circulation is shown in Fig. 1. Tropospheric air enters the stratosphere in the tropics. In the stratosphere it rises further upward and subsequently moves poleward downward at higher

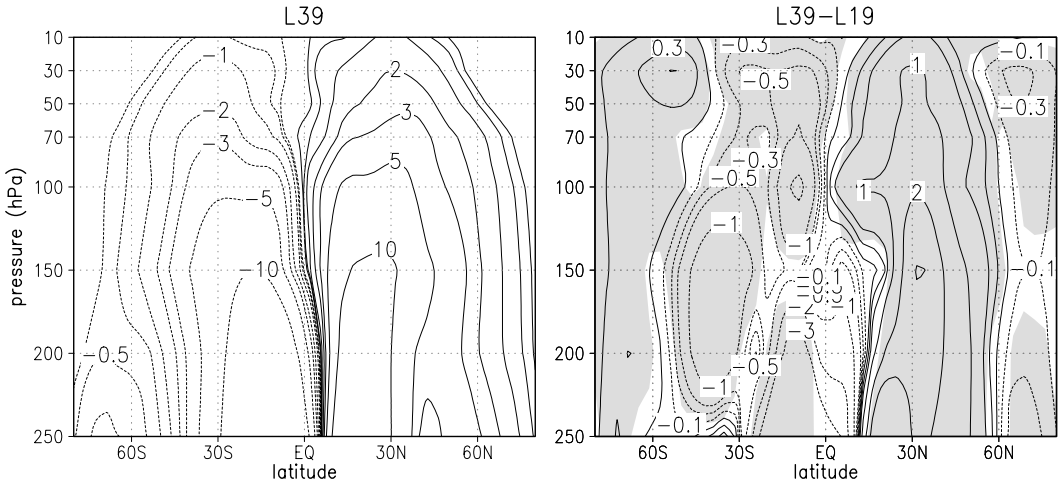

Fig. 1. Climatological mean residual mean meridional circulation in units of 10^9kg s^{-1} simulated by L39 (left), and difference between L39 and L19 (right). Within the shaded area the climatological mean values of both models differ at the 99.9% significance level (*t*-test).

latitudes. Equatorward of 60° north and south the climatological mean meridional mass circulation is significantly stronger in the L39 simulation than in the L19 model run. Poleward of 60° the circulation is weaker in L39 than in L19.

Dynamical differences between both models result in a different thermal structure. Therefore differences in the thermally defined tropopause between the models are expected (see World Meteorological Organization, 1986, for the thermal definition of the tropopause). Figure 2 shows the zonal and seasonal mean pressure at the thermal tropopause calculated from L39 and L19 results and determined from ECMWF analyses data for northern winter and summer. During all seasons the modelled tropopause pressure is lower than observed at polar and tropical latitudes (autumn and spring are not shown). In the subtropical transition zone it is higher than observed. The deviation between model and observational values at higher latitudes is attributable to the cold bias in the lower stratosphere of both models. Compared to the L19 simulation, the tropopause pressure is about 10–20 hPa lower in the tropics in the L39 results and it is somewhat higher in the subtropics and at polar latitudes, except in DJF in the polar southern hemisphere.

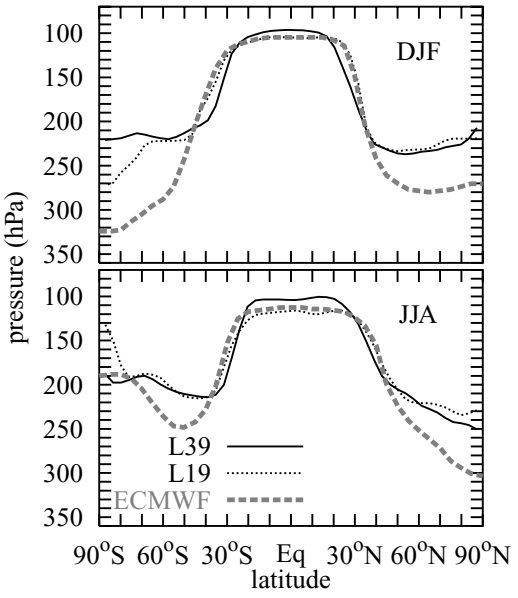

Fig. 2. Modelled and observed (ECMWF) zonal mean tropopause pressure for DJF (top) and JJA (bottom). Unit: hPa.

The tropopause pressure directly measures the stratospheric air mass, and hence the tropospheric air mass can be derived. During all seasons, except in northern winter, the stratospheric (tropospheric) air mass is lower (higher) in the L39 than in the L19 simulation.

3. Simulation set-up

The objective of this paper is to determine the impact of an increased vertical resolution on the transport and distribution of passive tracers. Therefore numerical experiments have been performed with L39 and L19 simulating the distributions of $^{14}CO_2$ and SF_6. The modelled tracer set-up is outlined in this section.

3.1. SF_6

SF_6 is initialised in both models with a globally uniform concentration field of 2.06 pptv on 1 January 1989 according to Denning et al. (1999). The period 1989–1993 (5 yr) is then simulated by running the model in climatological mode with observed sea surface temperatures and ice cover as boundary conditions. The surface emission flux of SF_6 is prescribed using estimates of monthly global emissions rates as proposed by Levin and Hesshaimer (1996). The SF_6 sources and their strengths are distributed geographically according to population density and electrical power usage as given in Denning et al. (1999) (Fig. 3). SF_6 is predominantly emitted in industrialised regions of the northern hemisphere, such as North America, Europe and South East Asia. There are no sinks in the troposphere and stratosphere. Ravishankara et al. (1993) assume that SF_6 is destroyed in the mesosphere as a result of electron attachment. As this sink is still very unclear it is not included in our model simulations. In the following, results with respect to SF_6 are presented from the last year of the model integration.

3.2. $^{14}CO_2$

Based on observed profiles of $^{14}CO_2$, Johnston (1989) constructed the zonally symmetric distribution of excess $^{14}CO_2$ for October 1963. This distribution represents only a rough estimate, because observations were scarce. Many injections occurred during the nuclear test series, and the total amount of radioactive material introduced is unclear. Error estimates for this distribution have not been given. In their recent study Hesshaimer and Levin (2000) systematically

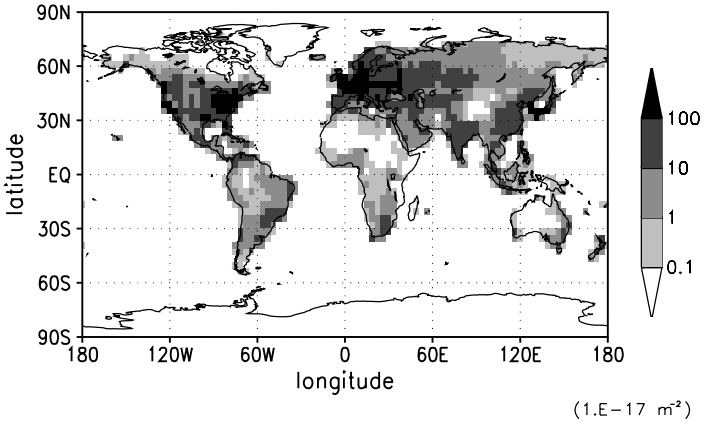

Fig. 3. Geographical distribution and density of SF_6 sources.

investigated the observational basis for this distribution, namely the stratospheric air samples collected during nuclear weapon tests and published in Health and Safety Laboratory reports. They determined an uncertainty of less than ±5% for the quarterly mean stratospheric $^{14}CO_2$ activity concentrations.

As the transport in the stratosphere is dominated by zonal winds it is assumed that bomb introduced $^{14}CO_2$ is distributed zonally homogeneous nine months after the series of bomb tests. The zonal mean distribution of excess $^{14}CO_2$ has been transferred to the different model grids of L19 and L39 (Fig. 4). Excess ^{14}C was predominantly released into the stratosphere of the northern hemisphere. Maximum $^{14}CO_2$ volume mixing ratios there exceeded 5000×10^{-18} mol mol^{-1} poleward of 30°N between 100 and 50 hPa. In the troposphere of the southern hemisphere the $^{14}CO_2$ concentration was lower than 300×10^{-18} mol mol^{-1}.

The temporal variation of the tropospheric $^{14}CO_2$ concentration is determined by exchanges with the ocean, the terrestrial biosphere, and the upper atmosphere, which includes variations in the natural production, anthropogenic emissions and radioactive decay. Following Hesshaimer et al. (1994) we apply a simple module for the global carbon cycle. We divide the biosphere into three carbon reservoirs (Fig. 5). The smallest represents leaves, fine roots and twigs. It has a capacity of 105 Pg(C), and its turnover time is 3 yr. The second reservoir, with a capacity of 675 Pg(C) represents branches, roots and tree–trunks. It takes 27 yr to replenish it fully. Soils store the largest amount of carbon. This reservoir is fed by both other

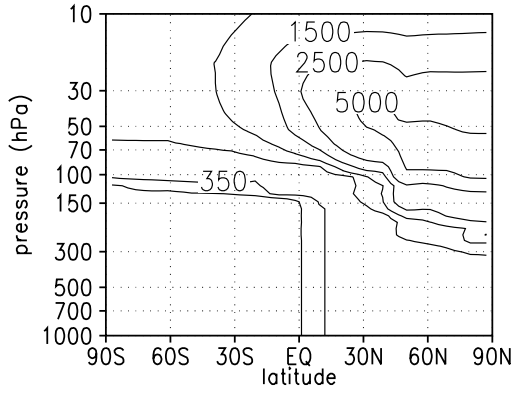

Fig. 4. Zonal mean distribution of excess $^{14}CO_2$ volume mixing ratio used as initial distribution for October 1963 in the L39 simulation. Isolines: 300, 350, 500, 850, 1500, 2500 and 5000×10^{-18} mol mol^{-1}.

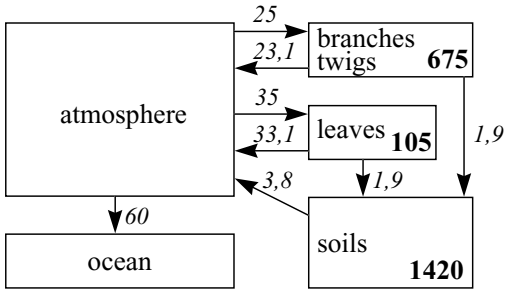

Fig. 5. Global carbon cycle and $^{12}CO_2$ fluxes [Pg(C)/yr] between the reservoirs, together with selected reservoir sizes (Pg(C)), used in the model simulations.

reservoirs. It has a capacity of 1420 Pg(C) with a turnover time of 375 yr. The $^{14}CO_2$ content of the oceans and the exchange with the terrestrial biosphere in the model depends on the $^{14}CO_2$ concentration at the surface level and the $^{14}CO_2$ content in each reservoir. It is proportional to the $^{12}CO_2$ surface fluxes as depicted in Fig. 5. This simple model for the global carbon cycle only accounts for long-term exchanges between each reservoir. Seasonal variations are not included.

In the model simulation only the distribution of excess $^{14}CO_2$, namely additional $^{14}CO_2$ from aboveground nuclear weapon tests, is modelled. Therefore the natural production of $^{14}CO_2$ and the emission due to other anthropogenic sources (e.g. fossil fuel combustion or release from light water reactors) are omitted. Oceans are able to store a vast amount of carbon. It is assumed that dissolved $^{14}CO_2$ is rapidly mixed downward. Therefore the flux back from the ocean into the atmosphere is neglected. $^{14}CO_2$ has a radioactive half-life of 5730 yr. As the $^{14}CO_2$-simulation period extends only over 10 yr the radioactive decay of $^{14}CO_2$ is negligible.

4. Results and comparison with observations

4.1. SF_6

4.1.1. Surface values. The observed SF_6 mixing ratio at the surface closely follows a quadratic function in time (Geller et al., 1997). The global trend of the modelled mixing ratio (in pptv) at the surface can be approximated by

$$\chi_0^{L39}(t) = 3.532 + 0.230t + 0.002t^2 \quad \text{for} \quad \text{L39} \quad (1)$$

$$\chi_0^{L19}(t) = 3.527 + 0.226t + 0.001t^2 \quad \text{for} \quad \text{L19} \quad (2)$$

with t being the time (in yr) relative to 1996. These curves have been determined by a least squares fitting procedure. The modelled monotonic increase is slightly faster than the growth rate that Geller et al. (1997) calculated from observational data. Using the same emission scenario Denning et al. (1999) also detected in their intercomparison study that the simulated surface mixing ratio was higher than observed for every model at all times of the year 1993 at all measurement sites. However, the differences between both curves remain small during this period (not shown).

In Fig. 6 the observed and the modelled SF_6 increases near the surface are depicted. The differences between both model simulations are very small, i.e. lower than 0.02 pptv. Therefore only the model values from the L39 simulation are plotted. As SF_6 is predominantly emitted at the surface of the northern hemisphere, the mixing ratio there is higher than in the southern hemisphere. The values at Izaña (28°N, 17°W) and Georg-von-Neumayer station (71°S, 8°W) differ by about 0.3 pptv. These features are nicely captured by both model versions.

Figure 7 displays meridional profiles of the surface SF_6 mixing ratio modelled by L39 and L19 for November 1993 together with observations taken over

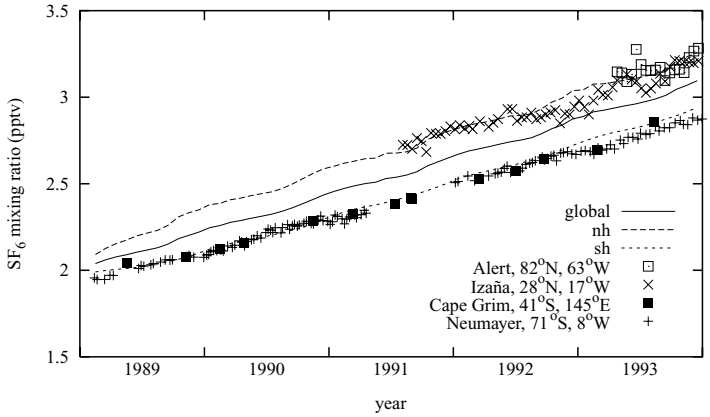

Fig. 6. Observed and modelled SF_6 mixing ratios near the surface. The observations are taken at Alert (⊡) Izaña (×), Cape Grim (■) and Georg von Neumayer (+). The curves represent global, northern hemisphere and southern hemisphere, respectively, means of the L39 model results.

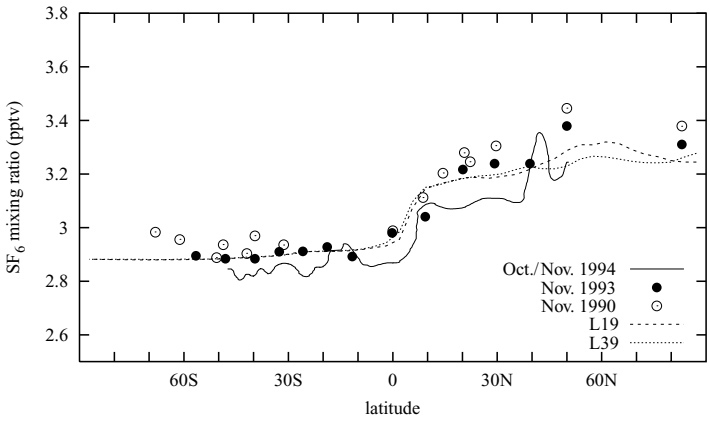

Fig. 7. Meridional profiles of the surface SF_6 mixing ratio over the Atlantic Ocean modelled by L39 (short dashed) and L19 in November 1993 (long dashed), and observed by UOH in November 1990 (⊙), and November 1993 (●) (Levin and Hesshaimer, 1996), and by NOAA in October/November 1994 (straight line) (Geller et al., 1997).

the Atlantic Ocean in November 1993 and November 1990 by the University of Heidelberg (UOH) (Levin and Hesshaimer, 1996), and in November 1994 by NOAA. The latter data have been adjusted to the UOH calibration scale (Geller et al., 1997). Additionally, all observational data have been scaled to November 1993 using the global growth rate given by Geller et al. (1997). We used the global growth rate to scale the observational data. In the years before 1994, the difference between the global growth rate and the growth rates at the surface of the northern and the southern hemisphere was less than 1%. The SF_6 concentration would differ only marginally if the hemispheric growth rates had been used to scale the data. Also in Fig. 7 the strong concentration gradient at the surface between the northern and the southern hemisphere is clearly visible. Compared to the observations both models realistically simulate this meridional profile. The model results differ only slightly in northern hemisphere midlatitudes. However, it is not possible to say how significant this result is without running an ensemble of simulations starting with differing meteorological conditions. We refrained from this due to the high computational expense.

On the whole, these results show that the geographical distribution of the sources and their strengths are chosen appropriately to yield realistic surface concentrations in the model simulations. To estimate the global performance of both models, the vertical distribution has to be evaluated.

4.1.2. Vertical distribution and profiles. In Fig. 8 the annual and zonal mean SF_6 distribution for 1993 simulated by L39 and the difference between both model simulations are shown. In the L39 simulation (Fig. 8, left) the SF_6 mixing ratio decreases with increasing altitude, ranging from more than 3.4 pptv at the surface of the northern hemisphere midlatitudes to values lower than 2.6 pptv poleward of 50°N above 50 hPa. Further, the SF_6 mixing ratio decreases monotonically from north to south in the whole troposphere. In the stratosphere however, at a given altitude the concentration is greatest in the tropics and decreases towards the poles. This structure reflects the residual mean meridional circulation (cf. Fig. 1). The difference between both model simulations is small in the troposphere (less than 1.5%), but in the stratosphere the model results differ systematically, especially in the northern hemisphere. Above the tropopause L39 simulates higher mixing ratios than L19, and the difference increases with altitude (Fig. 8, right). This difference can be explained by the stronger residual mean meridional circulation in the L39 simulation (Fig. 1).

To evaluate both models we show in Fig. 9 observed vertical profiles of the SF_6 mixing ratio from balloon soundings in Esrange (68°N), Aire sur l'Adour (44°N) and Hyderabad (17°N) (Harnisch et al., 1996; Patra et al., 1997), together with monthly mean results of both model simulations for December 1993. All observational vertical profiles have been scaled to December 1993. It has to be kept in mind that the reference growth rate is valid for the surface and not necessarily for the stratosphere. As the stratospheric SF_6 concentration lags behind the tropospheric concentration, the scaling would be more accurate if the age of air had been taken

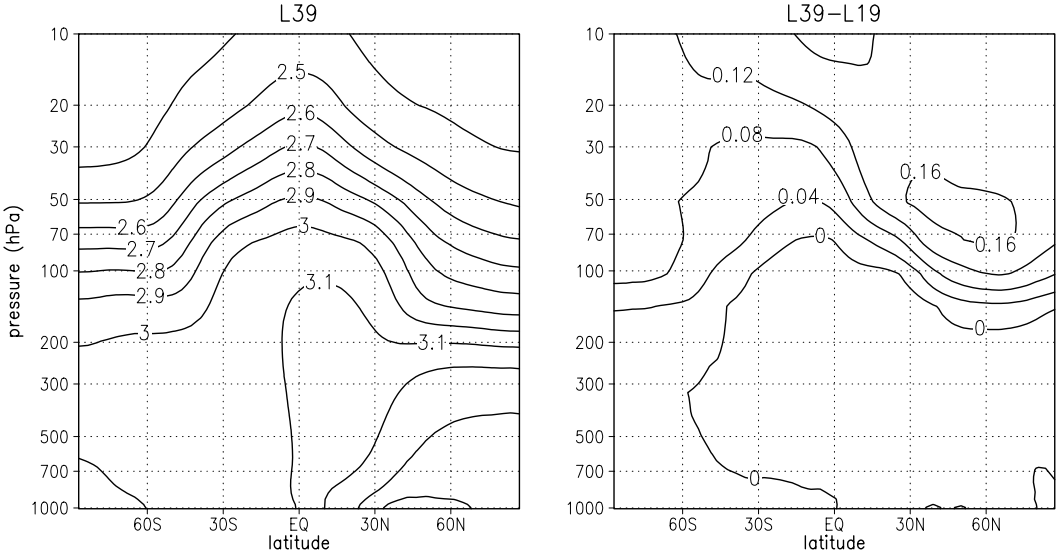

Fig. 8. Annual and zonal mean SF_6 mixing ratios modelled by L39 (left), and difference L39 minus L19 (right) for 1993. Unit: pptv.

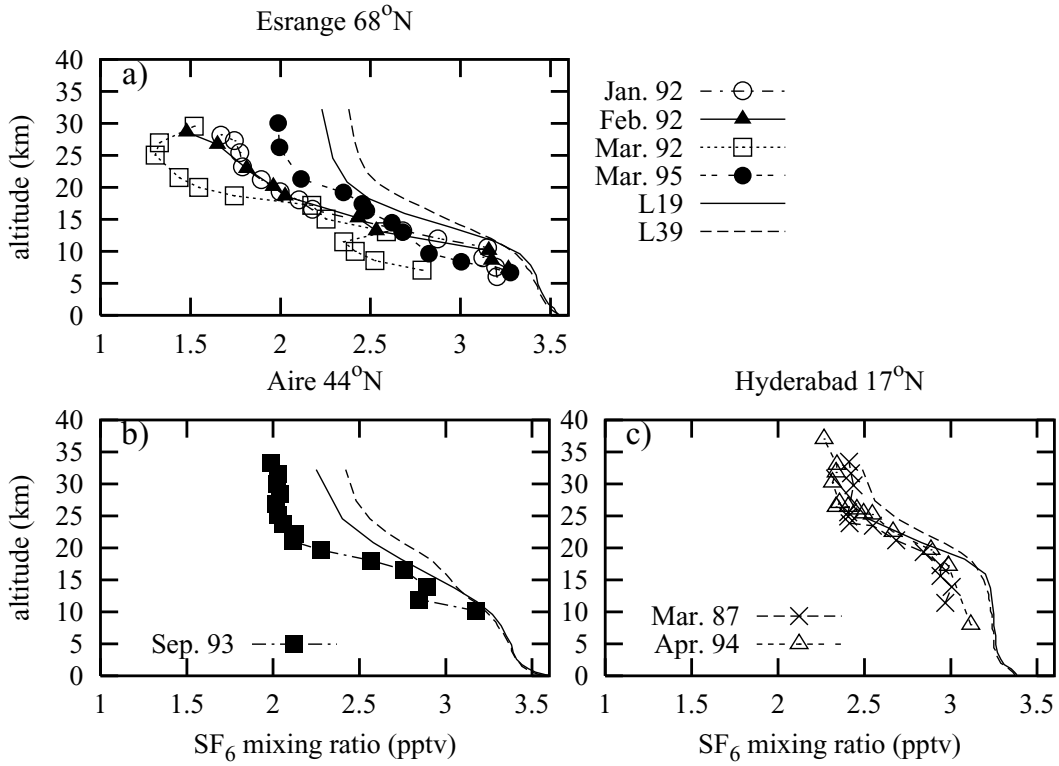

Fig. 9. Observed profiles of the SF_6 mixing ratio adjusted to December 1993 at different locations.

into account. However, the difference is again small. A SF_6 concentration of 1.5 pptv in the stratosphere in January 1992 [e.g. at the station Esrange (Fig. 9)] would increase to 1.9 pptv by December 1993 using solely the surface growth rate. Taking an age of 4 yr into account, the same concentration would rise to a slightly lower value of 1.8 pptv. In general, model results and observations are in good accordance below the tropopause. Above the tropopause, especially in 44°N and 68°N (Figs. 9a and b) the model simulations give higher (<10% in Aire) mixing ratios than observed. The difference in the SF_6 mixing ratio in the stratosphere between the L39 and the L19 simulation is smaller than the difference between both model results and the observations. The difference between model and observational values is greatest inside the polar vortex. This deviation can mainly be attributed to the chosen initial SF_6 distribution. The model simulations were started with a globally uniform mixing ratio of 2.06 pptv. In 1993 the model values in the stratosphere exceed the initial mixing ratios, because the supply of SF_6 from the troposphere increases with increasing surface emissions. Therefore the model values in the stratosphere exceed the observed concentrations, which are lower or about the same value than the initial SF_6 mixing ratio. Further, the modelled horizontal diffusion might be somewhat too high at a spectral resolution of T30. Increasing the horizontal resolution would reduce the diffusion due to the semi-Lagrangian advection scheme (Rasch and Williamson, 1990). In Hyderabad (Fig. 9c) the agreement between observed and modelled profiles is rather good.

4.2. $^{14}CO_2$

4.2.1. Regional results. The temporal evolution of the $^{14}CO_2$ mass due to nuclear weapon tests simulated by the L39 model is depicted in Fig. 10 for the total model atmosphere, troposphere, stratosphere, and northern and southern hemispheres. The structure of the L19 results is very similar and therefore not shown. After the initialisation in October 1963 the global $^{14}CO_2$ content in the atmosphere decreases with time, because $^{14}CO_2$ is absorbed by the oceans and the terrestrial biosphere. The decrease in time follows roughly an exponential curve with an e-folding time of 9 yr. The $^{14}CO_2$ content in the stratosphere decreases rapidly during the first year after the initialisation (by about 50%). It is dominated by the decrease of stratospheric $^{14}CO_2$ mass in the northern hemisphere. The e-folding times are 1.2 and 1.3 yr for the L39 and L19 simulation, respectively. For the period October to December 1963 the e-folding times of the stratospheric northern hemisphere $^{14}CO_2$ mass differ significantly between both model runs. The values are 1.6 and 1.0 for the L39 and L19 simulation, respectively. Thus during the first three months, where the vertical gradient in the $^{14}CO_2$ concentration is strongest, the mixing between the stratosphere and the troposphere is significantly weaker in L39 than in L19 due to weaker vertical diffusion. If this finding is transferred to chemical species like ozone, where chemical processes act to maintain strong vertical gradients, it can be concluded that the higher vertical resolution model L39 is more suited to preserve strong vertical tracer gradients. Once initialised $^{14}CO_2$ is only involved in atmospheric transport processes before it is taken up at the Earth's surface. Therefore the vertical gradients are smoothed during the following months and the e-folding times of both models converge.

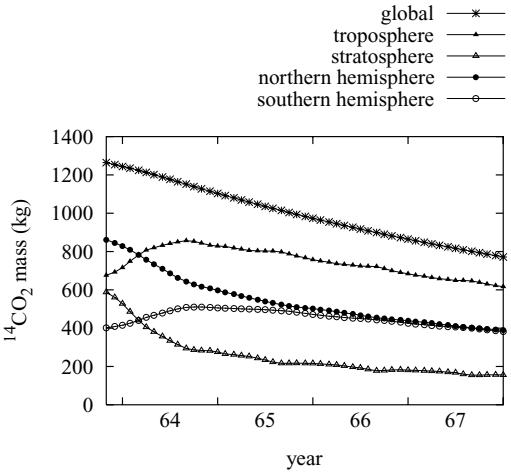

Fig. 10. Temporal evolution of the $^{14}CO_2$ mass for selected regions of the atmosphere modelled by L39.

In the troposphere the modelled $^{14}CO_2$ mass increases during the first year by about 26%. During this time the transport of $^{14}CO_2$ from the stratosphere into the troposphere is stronger than the uptake in the oceans and in the terrestrial biosphere. The temporal variation of stratospheric and tropospheric $^{14}CO_2$ masses can be explained by hemispheric differences of the seasonal variation of the tropopause height. In the global mean, the tropopause is higher in northern summer than in northern winter. Hence, the troposphere (stratosphere) encompasses a bigger (smaller)

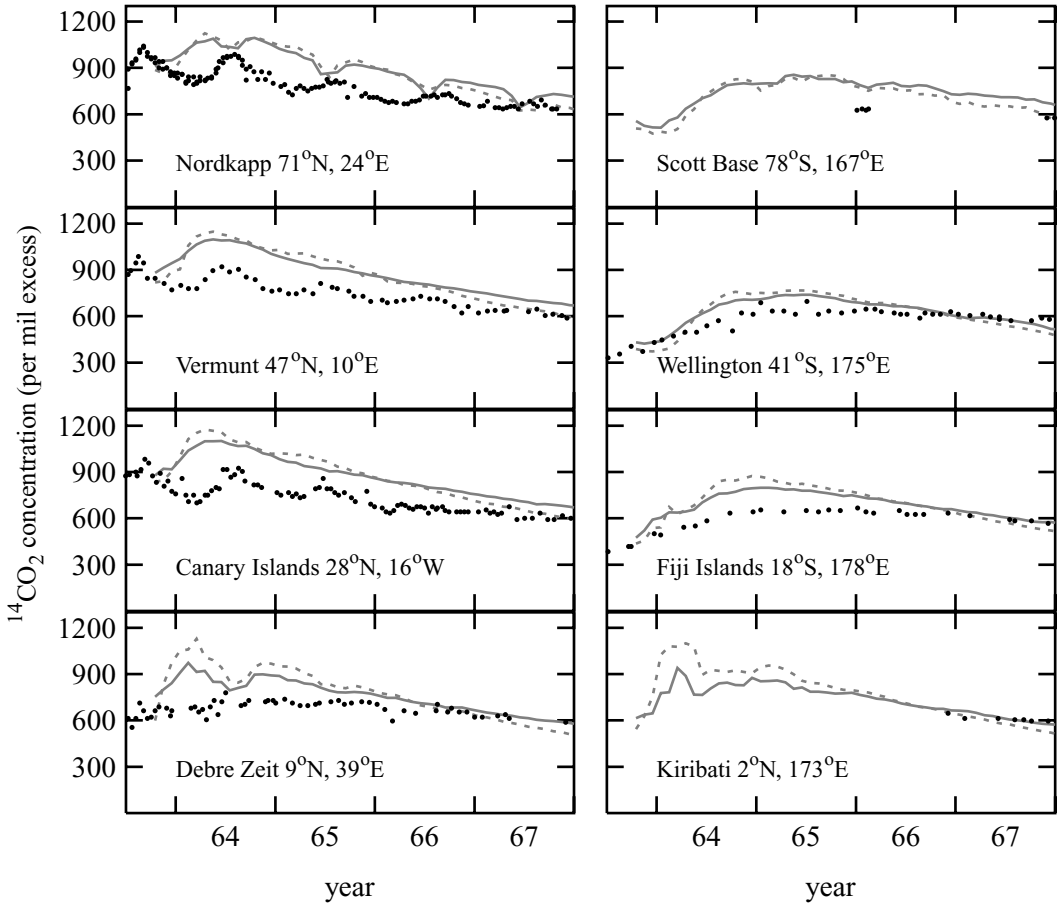

Fig. 11. Observed (dots) and modelled (L39 grey line; L19 dashed grey line) temporal evolution of the monthly mean $^{14}CO_2$ concentration at selected surface stations.

region and therefore the $^{14}CO_2$ mass during the summer months on the northern hemisphere is bigger (smaller) than during the winter months.

A comparison of the temporal evolution of the $^{14}CO_2$ mass in the northern and the southern hemisphere reveals that the fast decrease in the northern hemisphere can partly be explained by transport of $^{14}CO_2$ to the southern hemisphere. The hemispheric difference vanishes by the end of 1967. The annual mean interhemispheric exchange times are 0.83 and 0.86 yr for the L39 and the L19 simulation, respectively. In either model simulation the interhemispheric exchange time shows a minimum in summer (see also Kjellström et al., 2000). Later on, the $^{14}CO_2$ decrease in the atmosphere is a consequence of the uptake in the oceans and in the terrestrial biosphere.

4.2.2. $^{14}CO_2$ at the surface. In Fig. 11, modelled and observed temporal evolutions of bomb produced $^{14}CO_2$ are displayed for selected surface stations as relative deviations from the natural background value in per mil (‰). Kjellström et al. (2000) have already shown that the initial $^{14}CO_2$ concentration used in the model simulation for October 1963 is higher than observed at all stations (see their Fig. 16). As this deviation is only related to an erroneous initial $^{14}CO_2$ distribution, we have subtracted this offset in our comparison of modelled and observed $^{14}CO_2$ concentrations. Poleward of 28°N, maximum $^{14}CO_2$ activity concentrations at the surface were observed in the late summer of 1963. Further south, maximum concentrations occurred at later times, because the main input of bomb ^{14}C was in the northern hemisphere

stratosphere. The observed temporal difference of the occurrence of maximum $^{14}CO_2$ concentrations between Nordkapp and Wellington is 1.5 yr. Later the concentration decreased at all stations, because nuclear test series had ended, and $^{14}CO_2$ was taken up by oceans and the terrestrial biosphere.

Compared to the observations, the maximum concentrations at the surface in the model results occur at an earlier time and the concentration maximum is higher than observed. This overestimation can only be explained by a too strong downward transport in the initial stage of both model simulations. As air masses of northern hemispheric origin get mixed into the southern hemisphere with an interhemispheric exchange time of less than 1 yr in both models (see above), the overestimated downward transport in northern hemisphere midlatitudes therefore also contributes to the southern hemispheric surface concentrations and leads to an overestimation of the $^{14}CO_2$ surface concentration on the southern hemisphere. Reithmeier and Sausen (2001) substituted the semi-Lagrangian advection scheme of ECHAM4 by a Lagrangian module, using wind information in the original model coordinates and simulated the transport of $^{14}CO_2$. They found that the overestimated downward flux from the stratosphere into the troposphere is attributable to the numerical properties of the semi-Lagrangian transport scheme and not to model dynamics. However, it is clearly visible that the values of the first concentration maximum are lower in the L39 simulation than in the L19 simulation, especially in mid- and lower latitudes of the northern hemisphere. This suggests that the downward transport is less overestimated in the higher vertical resolution model.

The stratospheric SF_6 mixing ratio is larger in the L39 than in the L19 simulation due to the stronger residual mean circulation, in particular the branch with rising air in the tropics. Due to continuity reasons also the extratropical downward branch of this circulation is stronger in L39 than in L19. Thus the downward transport of $^{14}CO_2$ due to the residual circulation has to be stronger in L39 than in L19, and one would expect higher $^{14}CO_2$ surface concentrations in L39 than in L19. However, this is not the case during the first 2 yr after the initialisation. Until 1966 $^{14}CO_2$ surface concentrations are lower in L39 than in L19 for the following reason: During the first months after the initialisation the downward transport in the models is dominated by vertical diffusion. The residual circulation plays only a minor role, because the vertical velocity associated with it is relatively small (of the order of 0.3 mm s^{-1} at 100 hPa in the northern hemisphere). The strength of the vertical diffusion is positively correlated to the vertical concentration gradient and negatively correlated to the vertical resolution. It is obvious that the diffusive downward transport is significantly reduced with higher vertical resolution. Hence, the $^{14}CO_2$ surface concentrations are lower in L39 than in L19 in the beginning of the simulation. As the vertical gradient of the $^{14}CO_2$ concentration decays, vertical diffusion becomes less and less important compared to the residual circulation. In 1966 the stronger residual circulation in L39 has caught up the surface concentrations of the L19 simulation. Note that also in this case the difference between modelled concentrations is smaller than the difference between the model results and the observations.

The $^{14}CO_2$ concentration decreases faster than observed at all surface stations in the L19 simulation. Kjellström et al. (2000) related this behaviour to global sink terms, which are too strong. Figure 11 shows that this is also the case in the L39 simulation. However, in the L39 model the $^{14}CO_2$ concentration decreases more slowly at all stations in subsequent years than in the L19 simulation, e.g. at Nordkapp the observed e-folding time is 14.4 yr, the L19 model simulates an e-folding time of 6.0 yr and in the L39 simulation the e-folding time is 9.5 yr. In this respect the L39 simulations is more in accord with the observations.

Compared to the observations, the modelled seasonal variations at the stations Nordkapp, Vermunt, and on the Canary Islands show a lower amplitude and a phase lag (Nordkapp). The maximum surface concentration in northern hemispheric midlatitudes, observed in late summer 1964 at these stations, occurs at the beginning of 1964 in the model. This model feature can again only be explained by a too strong downward transport from the stratosphere, especially in midlatitudes in the initial stage of the simulation.

$^{14}CO_2$ is coupled with the global carbon cycle and therefore undergoes the same variations as CO_2. The exchange between the atmosphere and the terrestrial biosphere varies with time according to seasonal variations of plant growth. As a result, maximum CO_2 concentrations are observed in late winter and minimum CO_2 concentration in late summer with an amplitude of about 6 ppmv. In our model simulations we did not include seasonal variations of the $^{14}CO_2$ exchange between the atmosphere and the land biosphere, because they are negligible small: With a standard mixing ratio $^{14}CO_2/^{12}CO_2$ of 1.176 pptv the amplitude of the seasonal $^{14}CO_2$ cycle would be 7×10^{-18} mol mol^{-1} (cf.

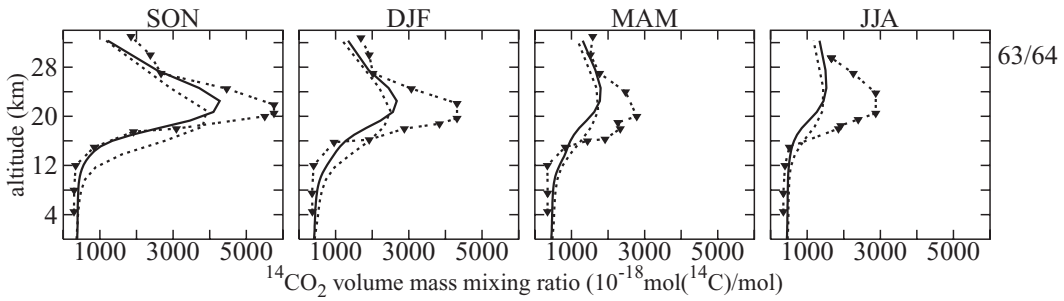

Fig. 12. Modelled (L39 grey line; L19 dashed grey line) and observed (triangles) profiles of the excess $^{14}CO_2$ mixing ratio in autumn, winter, spring, and summer at 31°N in the years 1963 and 1964.

Fig. 4). Thus, this simplification cannot explain the difference between observed and modelled seasonal $^{14}CO_2$ variations. Consequently, the $^{14}CO_2$ variation is dominated by seasonal variations of the downward transport from the stratosphere as well as fluctuations in horizontal transport of $^{14}CO_2$.

4.2.3. $^{14}CO_2$ vertical distribution. Figure 12 shows the temporal evolution of observed and modelled vertical profiles of the zonal mean $^{14}CO_2$ mixing ratio at 31°N. In autumn 1963 the maximum $^{14}CO_2$ mixing ratio is observed at 21 km altitude. The modelled maximum is about 2 km higher in the L39 simulation and its value is about 25% lower, whereas the L19 simulation captures the height of the initial $^{14}CO_2$ maximum, but the value is about 30% lower than observed. This discrepancy between observations and model results is due to the fact that both models are started in October 1963, and the modelled profiles show the mean value of October and November. The observations, however, are only available as the quarterly mean of September, October and November, with highest values observed in September. In the period autumn 1963 to summer 1964 the modelled maximum $^{14}CO_2$ concentrations are reduced by about 65%. The observed maximum decreases by 50%. Until autumn 1964 it is shifted upward by about 3 km in the model simulations due to the sink at the surface. In general the modelled values in the stratosphere are about 1.5–2 times lower than observed. In Fig. 12 it can also be seen that the downward transport of $^{14}CO_2$ in the L39 model is weaker in the initial stage of the simulation, and the sharp concentration gradient at the tropopause is better maintained (see SON 63/64 in Fig. 12) than in the L19 simulation. Hence, the L39 model simulation of $^{14}CO_2$ is more in accord with observations.

The modelled downward transport of $^{14}CO_2$ in the first months after the initialisation is stronger as observed, and the strong vertical concentration gradient above the tropopause is not maintained by the models to the same extent than observed. The reasons for this shortcoming are the downward transport, which is too strong especially in midlatitudes, and a tropopause which is higher than observed (Fig. 2). The latter deviation is attributable to the cold bias in the lower stratosphere of both models. As a consequence, bomb-produced $^{14}CO_2$ has been initialised partly in the troposphere where vertical transport and mixing is significantly higher than in the stratosphere. If this portion had been placed in the stratosphere, it would have been transported much more slowly towards the surface. Hence, $^{14}CO_2$ surface concentrations would have been lower.

5. Sensitivity of the stratospheric circulation to the position of the model top

The top level of both the L39 and the L19 model is centred at 10 hPa. This seems to be a rather low model top, especially for a study, where the stratospheric circulation plays such a an important role. To investigate how sensitive the stratospheric circulation is to the position of the model top, we have calculated the mean age of air from the SF_6 simulations of L39 and L19 and compare these results with the distribution of mean age derived from a simulation of SF_6 with MAECHAM4. The latter model is the middle atmosphere version of ECHAM4. Its top model level is centred at about 80 km. The set-up of the simulation with MAECHAM4 differs from our L39 and L19 study of SF_6. Manzini and Feichter (1999) started it with zero SF_6 concentrations in October 1970 and cover 15 yr and 3 months (cf. subsection 4.1).

As SF_6 does not have any sink in the stratosphere, the vertical structure of its mass mixing ratio, namely the decrease with increasing altitude, is dominated by the mass exchange rate between the troposphere and the stratosphere. The transport timescale of the exchange may be described by the mean age of the air mass. The concept of age, taking into account the statistical nature of air parcels was formally developed by Hall and Plumb (1994). Based on their work, Waugh et al. (1997), Hall and Waugh (1998), and Hall et al. (1999) derived the mean age of stratospheric air from chemical transport model simulations. The mean age of an air mass in the stratosphere is the lag time of the stratospheric response from the tropospheric mixing ratio (Schmidt and Khedim, 1991). The mean age of air has been calculated according to Volk et al. (1997), using the results of the last year of each SF_6 simulation for L39 and L19, i.e. 1993, and all 15 yr for MAECHAM4. The time taken for the global mean signal of the surface tracer concentration to reach the equatorial tropopause is 0.3 yr for L39 and 0.4 yr for L19 and MAECHAM4.

Figure 13 depicts the vertical age structure of all three models. The mean age is lowest in the lower tropical stratosphere and increases poleward and with increasing altitude. At a given pressure level the mean age is lowest in the L39 model. At the Equator above 100 hPa the mean age of the L39 and the MAECHAM4 simulations agree quite well, whereas it is higher in L19. At the poles below about 70 hPa, L19 and MAECHAM4 show similar values of mean age. Above 70 hPa the mean age is substantially lower in L39 and L19 compared to MAECHAM4.

The meridional gradient of mean age between the Equator and the Poles is tabulated in Table 1. Both the L39 and the L19 results show a higher gradient in the northern hemisphere than in the southern hemisphere at 100 and 50 hPa. Furthermore, it is generally lower in L39 than in L19. Compared to MAECHAM4 the meridional age gradient at 100 hPa is lower in L39 and higher in L19. At 50 hPa the MAECHAM4 simulation gives the highest meridional gradient of mean age. The vertical gradient of mean age between 100 and 30 hPa above the poles is similar in L39 and L19: it is 1.6 yr in the northern and 1.9 yr in the southern hemisphere. In MAECHAM4 it is 2.5 and 2.8 in the northern and southern hemisphere, respectively. In the tropics the values are 1.8, 2.4, and 1.8 for L39, L19, and MAECHAM4, respectively.

The age values of L39 are similar to the age distribution of the GISS model (Goddard Institute for Space Studies' Global Climate Middle Atmosphere model) shown in Hall and Waugh (1997) (their Fig. 1), whereas the L19 age distribution has slightly higher age values. Using a CTM covering the atmosphere up to 50 km, Waugh et al. (1997) determined a meridional age gradient which was twice as large as in L39 and L19 and even larger than in MAECHAM4. The air

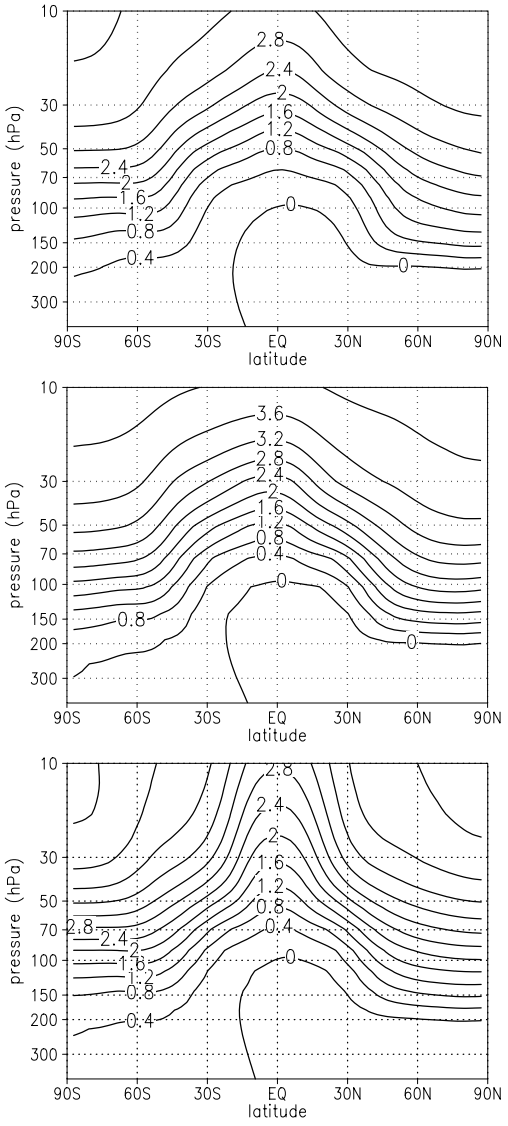

Fig. 13. Vertical structure of the mean age determined from SF_6 simulations with L39 (top), L19 (middle) and MAECHAM4 (bottom). Unit: yr.

Table 1. *Meridional gradient of mean age (yr) between the poles and the tropics for the 50 and the 100 hPa levels modelled by L39, L19, and MAECHAM4*

	100 hPa		50 hPa	
Model	NH	SH	NH	SH
L39	1.8	1.4	2.1	2.0
L19	2.2	1.9	2.3	2.1
MAECHAM4	2.0	1.7	2.6	2.6

mass at 20–30 km altitude (50–10 hPa) was 2 yr older (compared to L39 and L19) and 1 yr older (compared to MAECHAM4). The stratospheric age structure calculated from observed vertical SF_6-profiles also shows older air above the poles. Harnisch et al. (1996, 1998) determined an age of 5–10 yr for air masses in the polar vortex. These high values might be attributed to air masses with low SF_6 mixing ratios coming from high altitudes and sinking downward above the poles. As the top levels of both the L39 and the L19 model versions are centred at 10 hPa and no sink has been described, the mean age in the models has to be lower compared to these observations. One reason for the differences between models is that the horizontal concentration gradient between lower and higher latitudes might be underestimated due to the homogeneous initial SF_6 distribution in the L39 and L19 simulations, i.e. with an initial SF_6 concentration of 2.06 pptv the mean age is always lower than 4.1 yr. Another reason is that horizontal mixing is overestimated.

In a more recent work Hall and Waugh (1998) showed that despite the long lifetime of SF_6 its chemical destruction in the mesosphere is important for the mean age calculation from observations. Due to this sink, the vertical concentration gradients are higher than they would be for a perfectly inert tracer. Therefore the observed mean age is overestimated. Thus, if the mesospheric sink had been included in the model simulations, it is likely that the mean age would agree better with the observations. Hall and Waugh (1998) found that the overestimation is higher in the extratropics than in the tropics. Depending on the model used and prescribed sinks, the age at 68°N was overestimated up to 10% at 20 km and up to 65% at 30 km. Consistent with the results shown so far the mean age is lower in the L39 than in the L19 simulation. This is attributable to a stronger residual mean meridional circulation. The mean age and its vertical gradient in the tropics, and thus the upward transport velocity, are similar in the L39 and the MAECHAM4 simulations. However, the strong meridional gradient of mean age in the lower stratosphere cannot be achieved with either the L39 or the L19 for the following reasons: The initially global constant SF_6 concentration prevents higher age values above the poles, also the low top model level, which is centred at 10 hPa, might hamper a realistic stratospheric circulation.

6. Summary and conclusions

The impact of an increased vertical resolution on the transport and distribution of the passive tracers $^{14}CO_2$ and SF_6 has been investigated by means of numerical model simulations with two versions of ECHAM4, with the top level centred at 10 hPa but different vertical resolution: the standard model with 19 model layers and a higher-resolution version with 39 layers. Both models are able to reproduce the observed SF_6 concentrations in the troposphere. Only in the mid- and higher latitudes of the stratosphere do they simulate higher mixing ratios than observed. In the lower latitudes of the stratosphere the modelled SF_6 mixing ratios are in good agreement with observations. L39 generally calculates higher stratospheric mixing ratios than L19, and the difference increases with altitude. This difference between the modelled profiles has been attributed to the residual mean meridional circulation, which is stronger in L39 than in L19. The deviation of the model results from the observed vertical profiles is due partly to the relatively coarse horizontal resolution, which causes stronger horizontal mixing into higher latitudes (i.e. the polar vortex) and partly to the initialisation of SF_6 with a globally constant concentration. These findings are confirmed by the vertical gradient of mean age calculated from the SF_6 distribution, which is weaker in the L39 than in the L19 simulation. A lower vertical gradient of the mean age is caused by a stronger residual mean meridional circulation. A stronger mean meridional circulation is equivalent to a higher upward transport velocity in the tropics.

The comparison of modelled $^{14}CO_2$ surface concentrations and vertical profiles with observations has shown that an increased vertical resolution in the climate model ECHAM4 reduces the strength of stratosphere–troposphere exchange. Although the tropopause is higher in the L39 simulation than in L19 in the beginning of the simulation, and thus more

$^{14}CO_2$ is introduced into the troposphere, the $^{14}CO_2$ surface concentrations are lower. Therefore, L39 is more able to capture and maintain strong vertical gradients in tracer concentrations than L19. However, compared to observations the downward transport is still too strong even in the L39 simulation. As a further consequence of the differing tropopause, the volume of air occupied by the troposphere and stratosphere of both models differ. The difference in the tropopause height does not affect our conclusion that strong vertical gradients, which occur e.g. in the vicinity of the tropopause, can be better maintained by the L39 model than by L19.

Generally the differences between the L39 and the L19 results are smaller than between the model results and observations.

One might suspect that the model dynamics is responsible for the excessive downward transport. However, Reithmeier and Sausen (2001) showed that this is not the case. They simulated the transport of $^{14}CO_2$ with a Lagrangian advection model coupled to ECHAM4 using velocities in the original model coordinates. They found that the overestimated downward flux from the stratosphere to the troposphere is rather due to the numerical properties of the semi-Lagrangian transport scheme than due to incorrect model dynamics. Improvements with respect to the numerical properties of the semi-Lagrangian advection scheme could possibly be achieved by further increasing both the horizontal and the vertical resolution (Rasch and Williamson, 1990; Rasch and Lawrence, 1998).

Improvements in the stratospheric circulation might also be achieved by shifting the top model level to higher altitudes (see section 5).

Another possible influence factor, which has yet to be studied, is the cold bias in the lower polar stratosphere of ECHAM4. Improvements in the temperature structure would directly improve the location of the tropopause. It is possible that the cold bias might partly be a reason for the too strong downward transport. Land et al. (1999) compared the residual mean meridional mass flux simulated by the two model versions, and calculated from ECMWF reanalysis (ERA) data. However, they did not find any systematic relationship between cold bias and residual mean meridional mass flux. The climatological mean residual mean meridional mass flux calculated from ERA data is weaker in the southern hemisphere than the modelled mass flux. In the northern hemisphere the observed residual mass flux is slightly stronger than in the L19 results, but somewhat weaker than in the L39 results.

7. Acknowledgements

We are grateful to Ingeborg Levin from Institut für Umweltphysik, University of Heidelberg, Heidelberg, and Manfred Maiss from Max-Planck-Institut für Chemie, Mainz, for providing SF_6 data. G. Hoffmann from Laboratoire de Climat et de l'Environnement, Gif-sur-Yvette, provided the $^{14}CO_2$ surface module. We also thank Thomas Reichler for providing the zonal mean tropopause pressure calculated from ECMWF data. We are much indebted to Erik Kjellström from Department of Meteorology, Stockholm University, Stockholm, Claudia Timmreck and Martin Schultz both from Max-Planck-Institut für Meteorologie, Hamburg, and Bill Collins from The Met Office, Bracknell, for their constructive suggestions on a former version of this paper. We also thank two anonymous reviewers for helpful comments and suggestions. A large part of this work was carried out during the first author's stay at the Institut für Physik der Atmosphäre, DLR Oberpfaffenhofen.

REFERENCES

Andrews, D., Holton, J. and Leovy, C. 1987. *Middle atmosphere dynamics*. Academic Press, London.

Austin, J., Butchart, N. and Swinbank, R. 1997. Sensitivity of ozone and temperature to vertical resolution in a GCM with coupled stratospheric chemistry. *Q. J. R. Meteorol. Soc.* **123**, 1405–1431.

Boville, B. A. 1991. Sensitivity of simulated climate to model resolution. *J. Climate* **4**, 469–485.

Boville, B. and Randel, W. 1992. Equatorial waves in the stratospheric GCM: effects of the vertical resolution. *J. Atmos. Sci.* **49**, 785–801.

Denning, A. S., Holzer, M., Gurney, K. R., Heimann, M., Law, R. M. et al. 1999. Three-dimensional transport and concentration of SF_6 – A model intercomparison study (TransCom 2). *Tellus* **51B**, 226–297.

Feichter, J. and Lohmann, U. 1997. The atmospheric sulfur cycle in ECHAM-4 and its impact on the shortwave radiation. *Climate Dyn.* **13**, 235–246.

Geller, L. S., Elkins, J. W., Lobert, J. M., Clarke, A. D., Hurst, D. F. et al. 1997. Tropospheric SF_6: observed latitudinal distribution and trends, derived emissions and interhemispheric exchange time. *Geophys. Res. Lett.* **24**, 675–678.

Hall, T. M. and Plumb, R. A. 1994. Age as a diagnostic of stratospheric transport. *J. Geophys. Res.* **99**, 1059–1070.

Hall, T. M. and Waugh, D. W. 1997. Timescales for the stratospheric circulation derived from tracers. *J. Geophys. Res.* **102**, 8991–9001.

Hall, T. M. and Waugh, D. W. 1998. Influence of nonlocal chemistry on tracer distributions – Inferring the mean age of air from SF_6. *J. Geophys. Res.* **103**, 13327–13336.

Hall, T. M., Waugh, D. W., Boering, K. A. and Plumb, R. A. 1999. Evaluation of transport in stratospheric models. *J. Geophys. Res.* **104**, 18815–18839.

Harnisch, J., Borchers, R., Fabian, P. and Maiss, M. 1996. Tropospheric trends for CF_4 and C_2F_6 since 1982 derived from SF_6 dated stratospheric air. *Geophys. Res. Lett.* **23**, 1099–1102.

Harnisch, J., Bischof, W., Borchers, R., Fabian, P. and Maiss, M. 1998. A stratospheric excess of CO_2 – due to tropical deep convection?. *Geophys. Res. Lett.* **25**, 63–66.

Hesshaimer, V. and Levin, I. 2000. Revision of the stratospheric bomb $^{14}CO_2$ inventory. *J. Geophys. Res.* **105**, 11641–11658.

Hesshaimer, V., Heimann, M. and Levin, I. 1994. Radiocarbon evidence for a smaller oceanic carbon dioxide sink than previously believed. *Nature* **370**, 201–203.

Johnston, H. S. 1989. Evaluation of excess carbon 14 and strontium 90 data for suitability to test two-dimensional stratospheric models. *J. Geophys. Res.* **94**, 18485–18493.

Kinnison, D. E., Johnston, H. S., Weisenstein, D. and Yue, G. K. 1993. Radionuclides as exotic tracers. In: *The atmospheric effects of stratospheric aircraft: report of the 1992 models and measurements workshop* (eds. M. Prather and E. Remsberg). NASA Reference Publication 1292 Vol. III, Special Diagnostic Studies, NASA, Washington DC, USA, I-1-I-90.

Kjellström, E., Feichter, J. and Hoffmann, G. 2000. Transport of SF_6 and $^{14}CO_2$ in ECHAM4. *Tellus* **52B**, 1–18.

Ko, M. K. W., Sze, N. D., Wang, W.-C., Shia, G., Goldman A. et al. 1993. Atmospheric sulfur hexafluoride: sources, sinks, and greenhouse warming. *J. Geophys. Res.* **98**, 10499–10507.

Land, C., Ponater, M., Sausen, R. and Roeckner, E. 1999. *The ECHAM4/L39(DLR) GCM – Technical description and model climatology*. DLR–Forschungsbericht 1999–31, Deutsches Zentrum für Luft– und Raumfahrt Oberpfaffenhofen, Germany, 45 pp, ISSN 1434-8454. Also available electronically via *http://www.pa.op.dlr.de/echam/L39.html*.

Levin, I. and Hesshaimer, V. 1996. Refining of atmospheric transport model entries by the globally observed passive tracer distributions of ^{85}krypton and sulfur hexafluoride (SF_6). *J. Geophys. Res.* **101**, 16745–16755.

Lindzen, R. S. and Fox-Rabinovitz, M. 1989. Consistent vertical and horizontal resolution. *Mon. Wea. Rev.* **117**, 2575–2583.

Lohmann, U. and Roeckner, E. 1996. Design and performance of a new cloud microphysics scheme developed for the ECHAM general circulation model. *Climate Dyn.* **12**, 557–572.

Maiss, M., Steele, L. P., Francey, R. J., Fraser, P. J., Langenfelds, R. L. et al. 1996. Sulfur hexafluoride – A powerful new atmospheric tracer. *Atmos. Environ.* **30**, 1621–1629.

Manzini, E. and Feichter, J. 1999. Simulation of the SF_6 tracer with the middle atmosphere MAECHAM4 model: aspects of the large–scale transport. *J. Geophys. Res.* **104**, 31097–31108.

Marshall, S., Roads, J. O. and Oglesby, R. J. 1997. Effects of resolution and physics on precipitation in the NCAR Community Climate Model. *J. Geophys. Res.* **102**, 19529–19541.

Nydal, R. and Lövseth, K. 1983. Tracing bomb ^{14}C in the atmosphere 1962–1980. *J. Geophys. Res.* **88**, 3621–3642.

Olga, P., Persson, G. and Warner, T. T. 1991. Model generation of spurious gravity waves due to inconsistency of the vertical and horizontal resolution. *Mon. Wea. Rev.* **119**, 917–935.

Patra, P. K., Lal, S., Subbaraya, B. H., Jackman, C. H. and Rajaratnam, P. 1997. Observed vertical profile of sulphur hexafluoride (SF_6) and its atmospheric applications. *J. Geophys. Res.* **102**, 8855–8859.

Pope, V. D., Pamment, J. A., Jackson, D. R. and Slingo, A. 2001. The representation of water vapour and its dependence on vertical resolution in the Hadley Centre Climate model. *J. Climate* **14**, 3065–3085.

Rasch, P. J. and Lawrence, M. 1998. Recent development in transport methods at NCAR. In: *MPI workshop on conservative transport schemes* (ed. B. Machenhauer). Report No. 265, Hamburg, Germany, Max–Planck–Institut für Meteorologie, 65–75.

Rasch, P. J. and Williamson, D. L. 1990. Computational aspects of moisture transport in global models of the atmosphere. *Q. J. R. Meteorol. Soc.* **116**, 1071–1090.

Ravishankara, A. R., Solomon, S., Turnipseed, A. A. and Warren, R. F. 1993. Atmospheric lifetimes of long-lived halogenated species. *Science* **259**, 194–199.

Reithmeier, C. and Sausen, R. 2002. Attila – atmospheric tracer transport in a Lagrangian model. DLR–Institute für Physik der Atmosphäre Report No. 141, Oberpfaffenhofen, Germany, ISSN 0943–4771.

Roeckner, E., Arpe, K., Bengtsson, L., Brinkop, S., Dümenil, L. et al. 1992. Simulation of the present-day climate with the ECHAM model: impact of model physics and resolution. Report No. 93, Max-Planck-Institut für Meteorologie, Hamburg, Germany, 171 pp.

Roeckner, E., Arpe, K., Bengtsson, L., Christoph, M., Claussen, M. et al. 1996. The atmospheric general circulation model ECHAM-4: model description and simulation of present-day climate. Report No. 218, Max-Planck-Institut für Meteorologie, Hamburg, Germany, 90 pp.

Roeckner, E., Bengtsson, L., Feichter, J., Lelieveld, J. and Rodhe, H. 1999. Transient climate change simulations with a coupled atmosphere–ocean GCM including the tropospheric sulfur cycle. *J. Climate* **12**, 737–754.

Sausen, R., Feneberg, B. and Ponater, M. 1997. Climatic impact of aircraft induced ozone changes. *Geophys. Res. Lett.* **24**, 1203–1206.

Schmidt, U. and Khedim, A. 1991. In situ measurements of carbon dioxide in the winter Arctic vortex and at midlatitudes: an indicator of the "age" of stratospheric air. *Geophys. Res. Lett.* **18**, 763–766.

Senior, C. A. 1995. The dependence of climate sensitivity on the horizontal resolution of a GCM. *J. Climate* **8**, 2860–2880.

Shia, R.-L., Ko, M. K. W., Zou, M. and Kotamarthi, V. R. 1993. Cross-tropopause transport of excess ^{14}C in a two-dimensional model. *J. Geophys. Res.* **98**, 18599–18606.

Simmons, A. J., Burridge, D. M., Jarraud, M., Girard, C. and Wergen, W. 1989. The ECMWF medium-range prediction models: development of the numerical formulations and the impact of increased resolution. *Meteorol. Atmos. Phys.* **40**, 28–60.

Stendel, M. and Roeckner, E. 1998. Impacts of horizontal resolution on simulated climate statistics in ECHAM4. Report No. 253, Max-Planck-Institut für Meteorologie, Hamburg, Germany, 57 pp.

Timmreck, C., Graf, H.-F. and Feichter, J. 1999. Simulation of Mt. Pinatubo aerosol with the Hamburg climate model. *Theor. Appl. Climatol.* **62**, 85–108.

Tompkins, A. and Emanuel, K. A. 2000. The vertical-resolution sensitivity of simulated equilibrium tropical temperature and water-vapour profiles. *Q. J. R. Meteorol. Soc.* **126**, 1219–1238.

Tsuyuki, T. 1994. Impacts of increased vertical resolution in the stratosphere on dynamical extended–range forecasts. *J. Meteorol. Soc. Jpn.* **72**, 795–810.

Upstillgoddard, R. C. and Wilkins, C. S. 1998. The potential of SF_6 as a geothermal tracer. *Water Res.* **29**, 1065–1068.

Volk, C. M., Elkins, J. W., Fahey, D. W., Dutton, G. S., Gilligan, J. M. et al. 1997. Evaluation of source gas lifetimes from stratospheric observations. *J. Geophys. Res.* **102**, 25543–25564.

Waugh, D. W., Hall, T. M., Randel, W. J., Rasch, P. J., Boville, B. A. et al. 1997. Three-dimensional simulations of long–lived tracers using winds from MACCM2. *J. Geophys. Res.* **102**, 21493–21513.

Williamson, D. L. and Rasch, P. J. 1989. Two-dimensional semi-Lagrangian transport with shape-preserving interpolation. *Mon. Wea. Rev.* **117**, 102–129.

Williamson, D. L. and Rasch, P. J. 1994. Water vapor transport in the NCAR CCM2. *Tellus* **46A**, 34–51.

Williamson, D. L., Kiehl, J. T. and Hack, J. J. 1995. Climate sensitivity of the NCAR Community Climate Model (CCM2) to horizontal resolution. *Climate. Dyn.* **11**, 377–397.

World Meteorological Organization 1986. *Atmospheric ozone 1985*. Global Ozone Research and Monitoring Project Report No. 16, Geneva, Switzerland.